JOURNAL OF MATERIALS SCIENCE 30 (1995) 683–692

# A new data reduction scheme for the fragmentation testing of polymer composites

T. LACROIX, R. KEUNINGS*
*Centre for Systems Engineering and Applied Mechanics, Université Catholique de Louvain, Bâtiment Euler, B-1348 Louvain-la-Neuve, Belgium*

M. DESAEGER, I. VERPOEST*
*Department of Metallurgy and Materials, Katholieke Universiteit Leuven, de Croylaan 2, B-3001 Leuven, Belgium*

A new reduction scheme of fragmentation data for the derivation of interfacial mechanical properties in polymer composites is proposed. The scheme is based on a theoretical model that accounts for elastic load transfer and friction at the interface, as well as for the statistical nature of fibre strength. Interface mechanical behaviour is characterized by two independent parameters, namely the interface bond strength and interface frictional resistance. Derived values of the two interface properties are computed, such that they yield the best possible agreement between experimental and theoretical results for the evolution of fibre fragment aspect ratio and debonding ratio as a function of applied strain. Results are reported for carbon fibres embedded in an epoxy matrix, with different levels of fibre surface treatment.

## 1. Introduction

Several micromechanical methods, such as micro-indentation, pull-out and fragmentation tests, have been devised in recent years for the characterization of interface mechanical properties in polymer composites. As discussed in a recent review [1], it is often difficult to correlate the results obtained on the same fibre–matrix systems with different experimental techniques. The basic reason is the lack of appropriate data reduction schemes that would account in a sufficiently realistic manner for the complex physical mechanisms involved.

The present work is devoted to the development of an improved reduction scheme of fragmentation data. Representative applications of fragmentation testing of polymer composites are reported in [2]–[5]. In fragmentation testing, a single fibre is embedded in a matrix, and the specimen is subjected to a monotonically increasing tensile strain in the direction of the fibre axis. Load transfer to the fibre then develops through shear stresses at the fibre–matrix interface. Since the fibre failure strain is usually lower than that of the matrix, the fibre will progressively fracture into an increasing number of fragments as the applied strain increases. The fragmentation process will continue for higher applied strains, until a saturation level is reached. At saturation, the interfacial shear stresses are no longer capable of inducing further fracture of the fibre fragments.

In the traditional approach to reduction of fragmentation data, one measures the aspect ratio at saturation, $S_{sat}$, which is defined as the average fragment length at saturation reported to the fibre diameter, $d_f$. Interface mechanical behaviour is then described by means of a single shear stress parameter, $\tau_K$, using Kelly's model [6]

$$\tau_K = \frac{\sigma_f^{ult}}{2S_{sat}} \quad (1)$$

In this equation, $\sigma_f^{ult}$ denotes the average fibre tensile strength. Since fibre strength is strongly dependent on length, $\sigma_f^{ult}$ must be evaluated at the average saturation length, $L_{sat} = S_{sat} d_f$.

As noted previously by many authors (e.g. [1, 5]), characterization of the interface mechanical behaviour by means of a single $\tau_K$ parameter, though useful as a preliminary approach, cannot account for the complex processes taking place during the fragmentation process. In a recent paper [7], Favre and co-workers report the results of a computer simulation of the fragmentation process. The simulation is based on one-dimensional load transfer equations that allow for partial debonding at the interface between the fibre fragments and the matrix. Load transfer is assumed to continue to take place in the debonded zones, through a friction mechanism. Based on data for the interface bond strength derived from pull-out testing, as well as on appropriate values for the fibre–matrix friction coefficient, the computer simulation reported in [7] is able to predict the critical aspect ratio with good accuracy.

* To whom correspondence should be addressed.

0022–2461 

The data reduction scheme proposed in the present paper assumes that the interface mechanical behaviour is characterized by two independent parameters: the interface bond strength, $\tau_{deb}$, and the interface frictional resistance, $\tau_{fri}$. Along lines similar to [7], a computer simulation of the fragmentation process is developed based on one-dimensional load transfer models. The simulation predicts the evolution of the fibre fragment aspect ratio and debonding ratio as a function of applied strain. The derived interface properties, $\tau_{deb}$ and $\tau_{fri}$, are then computed such as to obtain the best possible agreement between experimental and simulated results for the fragment aspect ratio and debonding ratio.

The paper is organized as follows. Section 2 describes the theoretical models upon which the proposed data reduction scheme is based. In particular, the validity of simple one-dimensional load transfer models is assessed by means of detailed finite element computations. The data reduction scheme is described in Section 3. In the present paper, it is applied to carbon–epoxy specimens with different levels of fibre surface treatment. The experimental results needed as input to the reduction scheme are gathered in Section 4, while the results are reported and discussed in Section 5. Conclusions are drawn in Section 6.

## 2. Modelling approach

### 2.1. Load transfer models

The load transfer models used in this paper are extensions of classical shear lag theories [8, 9]. In that framework, the fibre is modelled as a circular cylinder of diameter, $d_f$, and initial length, $l_{init}$. Its behaviour is assumed linear elastic and isotropic. The fibre is embedded into a matrix phase of annular form and external radius, $R_m$. The matrix behaviour is modelled as isotropic, non-linear elastic. In view of the assumed problem geometry, stress and strain fields are axisymmetric about the fibre axis.

At low applied axial strain, $\varepsilon$, the fibre remains intact and the matrix's non-linear behaviour plays no role. Since the initial aspect ratio, $s_{init} = l_{init}/d_f$, is usually quite large, and since $l_{init}$ is equal to the specimen length, we can approximate the fibre axial stress, $\sigma_f$, and the interface shear stress, $\tau$, as

$$\sigma_f \approx E_f\varepsilon \qquad \tau = 0 \tag{2}$$

where $E_f$ is the fibre's Young's modulus.

At higher applied strain, the fibre will rupture and debonding will possibly develop at the interface between the fibre fragments and the matrix. In order to compute the axial stress, $\sigma_f$, and interface shear stress, $\tau$, for each fragment, the basic assumptions of shear lag theory [8] are used:

(i) dynamical effects are negligible;
(ii) the fibre axial stress vanishes at the ends of each fibre fragment;
(iii) there is no interaction between broken fibre fragments; and
(iv) the matrix tensile strain becomes equal to the applied strain, $\varepsilon$, at some radial distance, $R$, from the fibre axis.

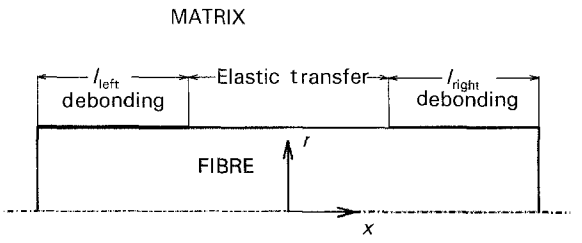


*Figure 1* Load transfer mechanisms and characteristic dimensions: $R$, radial distance; $x$, direction along fragment axis; $l$, length.

Regarding the latter assumption, finite element calculations show that $R = 25d_f$ is a reasonable choice [10].

Once debonding develops at the interface between a fibre fragment and the matrix, load transfer continues to take place through friction mechanisms. For a given applied strain, $\varepsilon$, it is assumed that the interface shear stress, $\tau$, is equal to a constant value, $\pm\tau_{fri}$, where debonding holds [8]. Here, $\tau_{fri}$ is referred to as the interface frictional resistance; where friction arises from the radial residual stress, $\sigma_{rad}^{res}$, and the differential Poisson's contraction stress, $\sigma^{Poisson}$. While $\sigma_{rad}^{res}$ can be viewed as independent of applied strain, it is assumed that $\sigma^{Poisson}$ is a linear function of $\varepsilon$. Thus

$$\tau_{fri} = \mu|\sigma_{rad}^{res} + \sigma^{Poisson}| = c_1 + c_2\varepsilon \tag{3}$$

where $\mu$ is a friction coefficient, and the $c_i$'s are positive material constants that are independent of applied strain.

Fig. 1 illustrates the load transfer mechanisms for a particular fibre fragment of length, $l$, and aspect ratio, $s = l/d_f$. In the general case, debonding develops over lengths, $l_{left}$ and $l_{right}$, from the two fragment ends; while the interface is intact in the central region. For each fragment, the debonding ratios, $m_{left} = l_{left}/(l/2)$, $m_{right} = l_{right}/(l/2)$, and the mean debonding ratio, $m = (l_{left} + l_{right})/l$ are defined.

Three particular cases of Fig. 1 are covered by classical shear lag theories. When perfect adhesion holds over the whole fragment length ($l_{left} = l_{right} = m = 0$), the stress distribution is given by Cox's model [11], and it can be said that load transfer is elastic. The second particular case, referred to as symmetric partially elastic, assumes that debonding occurs symmetrically over only a fraction of the fragment length ($l_{left} = l_{right} < l/2$, and $0 < m < 1$). In this case, load distribution is described by Piggott's equation [8, 12]. Finally, the opposite limit to adhesion over the entire fragment length is total debonding ($l_{left} + l_{right} = l$, or $m = 1$). This case is described by Kelly's model at saturation [6]. Both Kelly's and Cox's models can be viewed as asymptotic limits of Piggott's equation [9].

The general load transfer conditions of Fig. 1 involve partial debonding that is non-symmetric about the fragment centre. For a given applied strain, $\varepsilon$, the axial fibre stress, $\sigma_f$, and interface shear stress, $\tau$, in a fragment of length, $l$, are computed using extensions of the classical shear lag models. Equilibrium considerations yield the following stress distributions in the

central region of the fragment where perfect adhesion holds

$$\sigma_f = E_f\varepsilon + a\sinh(2nx/d_f) + b\cosh(2nx/d_f) + \sigma_f^{res} \quad (4)$$

$$\tau = -\frac{n}{2}[b\sinh(2nx/d_f) + a\cosh(2nx/d_f)]$$

with

$$n^2 = \frac{E_m(\varepsilon)}{E_f(1+\nu_m)\ln(2R/d_f)} \quad (5)$$

Here, $E_m$ is the matrix's secant Young's modulus, $\nu_m$ is the matrix's Poisson's coefficient, $a$ and $b$ are integration constants, and $\sigma_f^{res}$ is the fibre's axial residual stress. The coordinate $x$ is measured along the fragment axis, with the origin located at the middle of the fragment. Equations 4 and 5 hold in the elastic region $(m_{left} - 1)\frac{l}{2} \leqslant x \leqslant (1 - m_{right})\frac{l}{2}$. Continuity of the axial stress, $\sigma_f$, at both ends of the elastic region provides two relations for computing $a$ and $b$.

In the two regions where debonding occurs, equilibrium arguments yield the following stress distributions. For $-\frac{l}{2} \leqslant x < (m_{left} - 1)\frac{l}{2}$

$$\sigma_f = 2\tau_{fri}(l - 2x)/d_f + \sigma_f^{res}$$
$$\tau = -\tau_{fri} \quad (6)$$

while the result for $(1 - m_{right})\frac{l}{2} < x \leqslant \frac{l}{2}$ is

$$\sigma_f = 2\tau_{fri}(l + 2x)/d_f + \sigma_f^{res}$$
$$\tau = \tau_{fri} \quad (7)$$

The computation of the debonding ratios, $m_{left}$ and $m_{right}$, is performed in an iterative way, taking into account the history of the fragmentation process. For a given applied strain, the stresses $\sigma_f$ and $\tau$ must first be computed in the elastic region by means of Equation 4, using values of $m_{left}$ and $m_{right}$ determined for the previous strain increment. If the interface shear stress, $|\tau|$, evaluated at the junction between the elastic and debonded regions, i.e. at $x = (m_{left} - 1)\frac{l}{2}$ and $x = (1 - m_{right})\frac{l}{2}$, is smaller than $\tau_{deb}$, it can be concluded that debonding has not developed further during the current strain increment, and the values of $m_{left}$ and $m_{right}$ are kept unchanged. On the other hand, if the above conditions are violated, new values for $m_{left}$ and/or $m_{right}$ must be computed. This is achieved by specifying that the shear stress, $\tau$, in Equation 4 reaches the interface bond strength, $\tau_{deb}$, at the junction(s) between the elastic and debonded regions

$$|\tau|_{x=(m_{left}-1)\frac{l}{2}} = \tau_{deb},\ |\tau|_{x=(1-m_{right})\frac{l}{2}} = \tau_{deb} \quad (8)$$

The resulting non-linear equations are solved numerically by means of a standard iterative procedure. A schematic of typical stress results is shown in Fig. 2.

The inputs to the above load transfer equations are the applied strain, $\varepsilon$, the fibre's properties, $E_f$ and $\nu_f$, the matrix's properties, $E_m(\varepsilon)$ and $\nu_m$, the fibre's axial residual stress, $\sigma_f^{res}$, the geometrical parameters $l$, $d_f$ and $R$, and the interface's properties, $\tau_{deb}$ and $\tau_{fri}$.

In the data reduction scheme described below, the same basic equations are used to derive the interface frictional resistance, $\tau_{fri}$, and the interface bond strength, $\tau_{deb}$, from experimental fragmentation data.

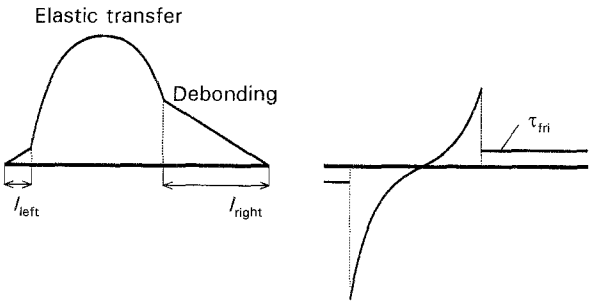


*Figure 2* Schematic distribution of axial fibre stress, $\sigma_f$, and interface shear stress, $\tau$, according to the non-symmetric, partially elastic model.

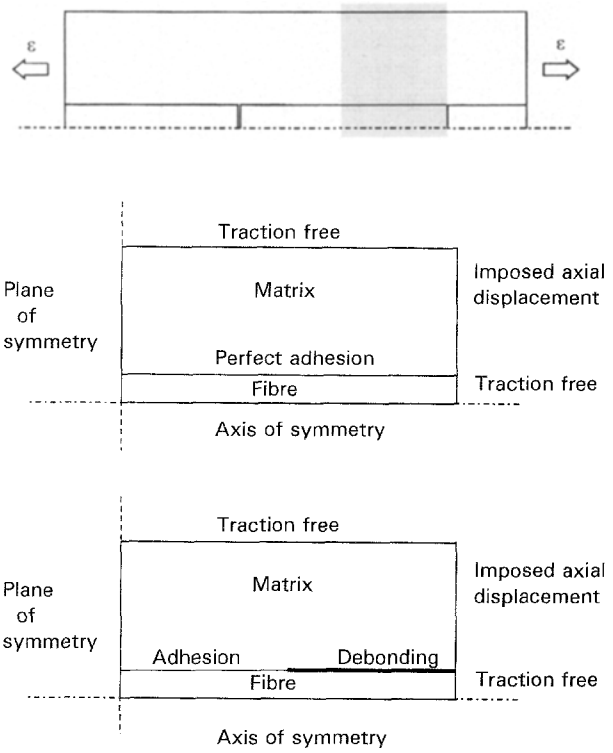


*Figure 3* Geometry of the finite element problem (shaded region), and boundary conditions for perfect adhesion and symmetric partial debonding.

## 2.2. Finite element validation

One should keep in mind that shear lag theories provide only one-dimensional approximations of the actual complex stress and strain fields developing in the fragmentation specimen. It is thus necessary to assess the validity of the above load transfer equations by means of more advanced, but also much more expensive, computational tools.

The stress distributions obtained with the one-dimensional load transfer models of Section 2.1 have been compared to detailed finite element calculations. The finite element problem is axisymmetric about the fibre axis. As shown in Fig. 3, half of a fibre fragment is analysed, together with the surrounding matrix. Two cases are considered: perfect adhesion at the interface, and symmetric partial debonding with a specified debonding ratio. Fig. 3 shows the corresponding boundary conditions. The material and geometrical data used in the computations correspond to the carbon–epoxy specimen characterized in Section 4. The matrix external radius, $R_m$, is equal to $25d_f$. Consistent

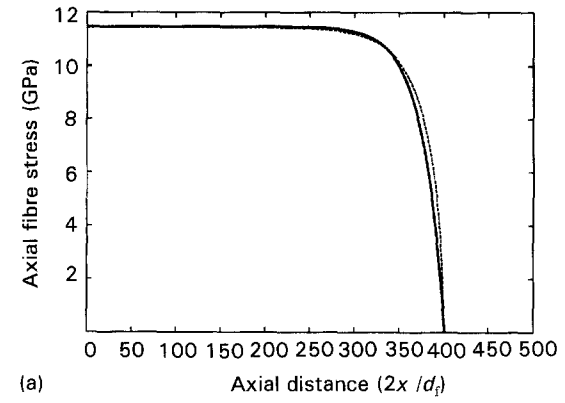


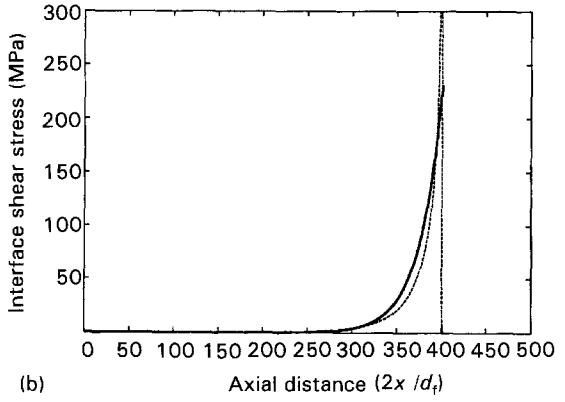


*Figure 4* (a) Axial fibre stress, $\sigma_f$, and (b) interface shear stress, $\tau$, (perfect adhesion): one-dimensional results (continuous lines) and finite element predictions (dashed lines).

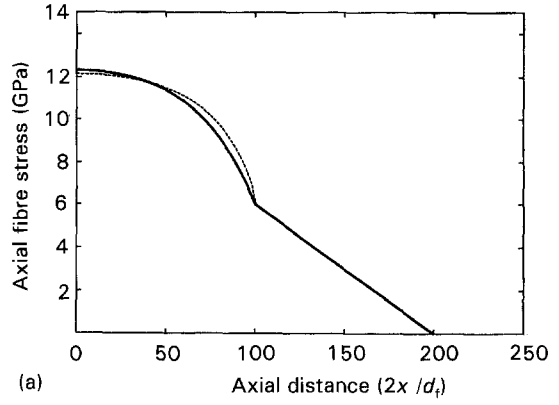


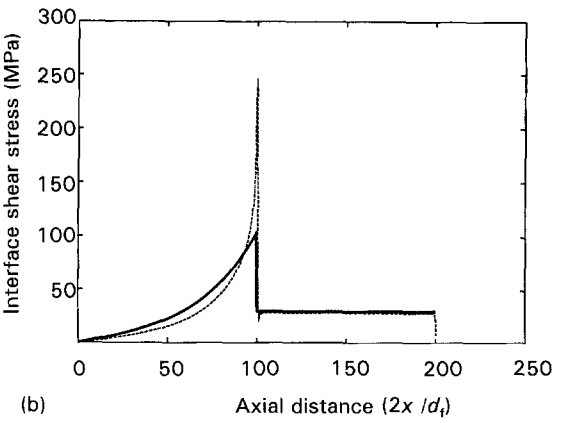


*Figure 5* (a) Axial fibre stress, $\sigma_f$, and (b) interface shear stress, $\tau$, (symmetric partial debonding): one-dimensional results (continuous lines) and finite element predictions (dashed lines).

with the one-dimensional models of Section 2.1, the finite element analysis assumes linear elastic behaviour of the fibre and the matrix; the matrix rigidity is given by the secant Young's modulus, $E_m(\varepsilon)$, evaluated at the applied strain.

Now, first consider the case of perfect adhesion at the interface. The applied strain, $\varepsilon$, is set to 0.037, and the fibre aspect ratio is 400. These values are typical of the experimental conditions when perfect adhesion is observed to hold (Section 4). Fig. 4 compares finite element and one-dimensional results for the axial fibre stress, $\sigma_f$, and the interface shear stress, $\tau$; agreement is excellent for $\sigma_f$. It is also quite good for $\tau$, except in a small region near the fibre end. There, very high values of the shear stress develop in the finite element results due to the discontinuity in boundary conditions. In reality, plastic deformations will take place in that region, and actual stress levels will be reduced. This is not taken into account in the present analysis.

Results for the case of partial debonding are shown in Fig. 5. Here, a symmetric debonding length, $l_{right} = l_{left} = l/4$ is specified. In the debonded zone, the finite element analysis enforces continuity of the radial displacement and sets the interface shear stress to a specified uniform value, $\tau_{fri} = 30$ MPa. Consistent with the experimental conditions reported in Section 4, the applied strain is set to 0.042, and the fragment aspect ratio to 200.

Here again, agreement is excellent for $\sigma_f$. It is also quite good for $\tau$, except in a small neighbourhood of the discontinuity between the elastic and debonded zones, where high stress levels are predicted by the finite element analysis.

It can be concluded from these finite element calculations that the rather simple load transfer models of Section 2.1 capture the main features of stress transfer and can be used with confidence in the analysis of the fragmentation test.

## 2.3. Fibre strength

The final ingredient needed to deduce fragmentation data is a model for fibre strength. In view of the complex mechanisms involved in fibre tensile fracture, one often uses a statistical description of strength. In the present work, fibre strength is modelled by means of a two-parameter Weibull distribution [13, 14]. According to this model, the probability that a fibre of length, $l$, breaking at a stress lower than $\sigma$ is given by

$$P(\sigma; l) = 1 - \exp[-l(\sigma/\sigma_0)^m] \quad (9)$$

The parameters m and $\sigma_0$ are material constants independent of fibre length. Equation 9 yields the average fibre strength

$$\overline{\sigma_f^{ult}}(l) = \sigma_0 l^{-1/m} \Gamma\left(1 + \frac{1}{m}\right) \quad (10)$$

where $\Gamma$ is the gamma function.

Consistent with the Weibull statistics, the fibre with initial length, $l_{init}$, is modelled as a linear chain of $n$ subsegments of length, $l_n = l_{init}/n$. Random values

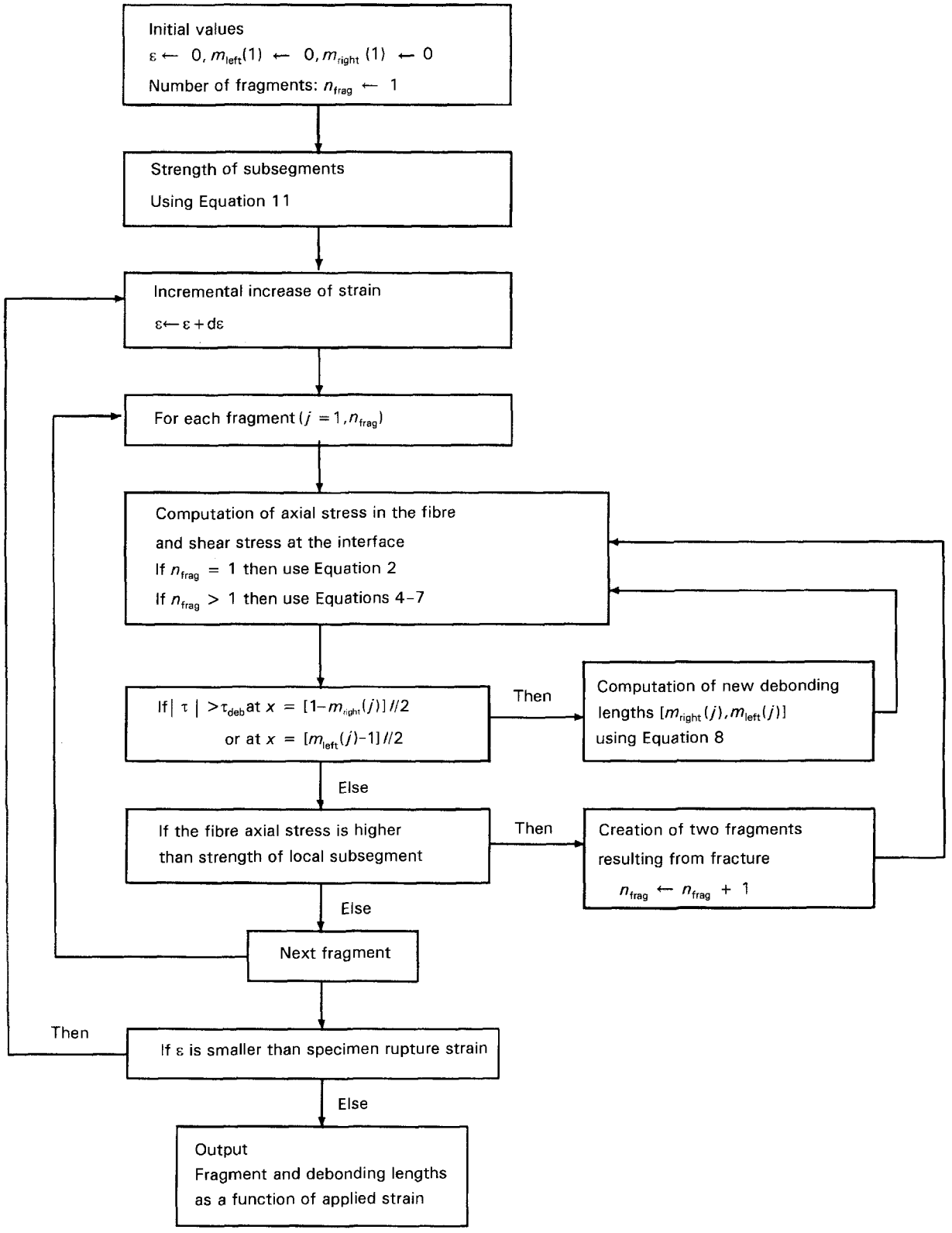


*Figure 6* Computer simulation of the fragmentation test.

for the strength $\sigma_f^{ult(i)}$ of subsegment $i (i = 1, 2, \ldots, n)$ are obtained by inversion of Equation 9. Thus

$$\sigma_f^{ult(i)} = \sigma_0 l_n^{-1/m} \left\{ \ln \left[ \frac{1}{1 - ran(i)} \right] \right\}^{1/m} \quad (11)$$

where ran($i$) denotes a random number uniformly distributed between 0 and 1. In the simulations reported below, $n$ is set to 2000 so that each fibre fragment contains at least 50 subsegments at the end of the fragmentation process.

## 3. Data reduction scheme

The proposed data reduction scheme consists of deriving the interface properties, $\tau_{deb}$ and $\tau_{fri}$, that will give the best agreement between experimental and computer simulated fragmentation data. Since $\tau_{fri}$ takes

the assumed form $c_1 + c_2\varepsilon$, a three-parameter optimization problem must be solved.

More precisely, for a series of specified values of $\tau_{deb}$, $c_1$ and $c_2$, evolution of the average fragment aspect ratio, $S$, and average debonding ratio, $M$, are computed as functions of applied strain, using the theoretical models of Section 2. An optimization technique then gives the derived interface properties that yield the best agreement between experimental and simulated results for $S$ and $M$.

The main steps of the computer simulation are illustrated in Fig. 6. Initially, there is only one fragment of length, $l_{init}$. It is assumed that perfect adhesion holds along the initial fragment. The fibre is modelled as a chain of $n$ subsegments, and each subsegment is given a random strength using Weibull statistics [11]. The applied strain, $\varepsilon$, is then increased incrementally.

For a given strain, the number of fibre fragments, their aspect ratio, their debonding ratio and the distribution of axial stress, $\sigma_f$, and interface shear stress, $\tau$ can be determined iteratively. In each fragment, elastic transfer is assumed to hold until the interface shear stress reaches the interface bond strength, $\tau_{deb}$. Debonding is then allowed to develop over part of the fragment; the extent of debonding is computed by means of the load transfer equations of Section 2.1. Rupture of a fragment is predicted as soon as the axial stress, $\sigma_f$, within a local subsegment reaches the subsegment strength. The fragment is then divided accordingly, and load transfer is recomputed for the newly produced fragments. Once this iterative scheme has converged, the applied strain is incremented. The simulation ends when the applied strain has reached the experimental rupture strain of the fragmentation specimen.

For specified values of $\tau_{deb}$ and $\tau_{fri}$ (the latter being determined by the constants $c_1$ and $c_2$ in Equation 3), the evolution of the fragment aspect ratio and mean debonding ratio are thus computed as a function of applied strain. Average $S$ and $M$ values of these two quantities are taken over all fragments produced at each strain level. An optimization procedure is then invoked to derive the interface properties, $\tau_{deb}$ and $\tau_{fri}$, that yield the best agreement between the computer predictions for $S$ and $M$, and the corresponding experimental results, $S_{exp}$ and $M_{exp}$. To this end, an expression is minimized of the form

$$\sum_{i=1}^{n_{exp}} [w_S^{(i)} |S(\varepsilon_i) - S_{exp}(\varepsilon_i)| + w_M^{(i)} |M(\varepsilon_i) - M_{exp}(\varepsilon_i)|] \quad (12)$$

Here, the sum is taken over a number, $n_{exp}$, of strain levels, $\varepsilon_i$, for which experimental data are available. The symbols $w_S^{(i)}$ and $w_M^{(i)}$ denote positive constants. Their values can be set such as to put more weight on specific data points. For example, more weight is assigned to the $S$ results at high applied strains compared with those at low strains, in view of the lower level of scatter in the experimental data [10].

The overall optimization procedure is repeated (typically five times), such as to assign different random strengths to the subsegments. The final derived interface properties are averages of the results obtained in the different optimization runs. A complete reduction of fragmentation data takes the order of six CPU hours on a DEC 5000/200 engineering workstation.

## 4. Experimental input data

The above data reduction scheme has been applied to four different types of carbon fibres embedded in an epoxy matrix. This section gathers the experimental data needed as input to the computer code. Details on the experimental procedures used to obtain the data are given in [15, 16].

### 4.1. Materials data

The matrix used in these fragmentation experiments is the resin LY5052 from Ciba Geigy. Its tensile stress–strain curve and the corresponding secant Young's modulus, $E_m(\varepsilon)$ were measured, Fig. 7. In the sequel, a value of 0.38 is used for the matrix's Poisson's ratio, $\nu_m$.

The tested fibres are the IM 43–750 intermediate modulus carbon fibres produced by Courtaulds Ltd. They distinguish themselves by the different levels of oxidative surface treatment they have undergone at the end of the production line. The exact nature and conditions of the surface treatment are proprietary. The 100% standard surface treatment (SST) fibres have received the so-called standard level of surface treatment, while the 0% SST fibres are untreated.

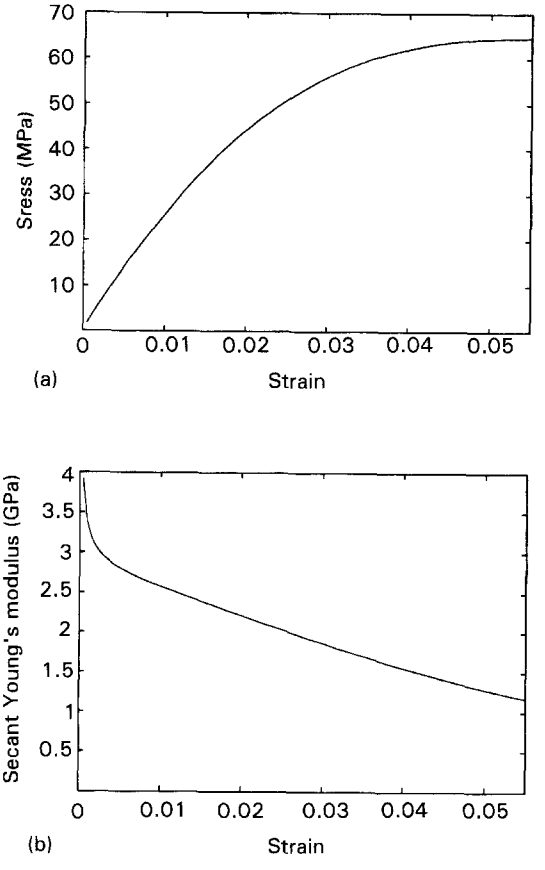


*Figure 7* (a) Tensile stress–strain curve, and (b) secant Young's modulus of the LY5052 epoxy matrix.

The 10 and 50% SST fibres received a corresponding fraction of the standard treatment level.

The tensile strength of the four carbon fibres have been characterized by means of the two-parameter Weibull statistical model [9]. The results are listed in Table I. With the exception of the 10% SST data, the surface treatment is observed to induce a small continuous decrease in tensile strength. For large gauge lengths, the 10% SST fibres are stronger than the 0% SST fibres, while the opposite is observed for short gauge lengths.

The (longitudinal) Young's modulus, $E_f$, was found independent of the level of surface treatment; its measured value is 310 GPA. In the sequel, a value of 0.2 is used for the fibres' Poisson's ratios, $\nu_f$. The fibres' diameter, $d_f$, is 4.8 μm, while their initial length, $l_{init}$, is 10 mm.

## 4.2. Fragmentation data

Fragmentation data have been obtained on dog-bone specimens prepared by using silicon moulds [15]. In order to ensure alignment of the fibre in the matrix, single fibres taken out of a fibre bundle were placed on a metal frame before positioning in the silicon moulds. The weight of the frame enables control of fibre tension and hinders fibre buckling due to residual thermal stresses. This preparation step is crucial. Indeed, it has been shown that parameters such as applied fibre tension, type of silicon mould and choice of appropriate curing cycle, play an important role on the fragmentation process [15]. Indeed, they control the levels of residual thermal stresses present in the specimen. In view of the fact that the same preparation procedure was used for all tested specimens, it shall be assumed in the sequel that the residual stresses have identical values for all cases.

TABLE I Weibull parameters of the four tested fibres

| SST (%) | $m$ | $\sigma_0$ (GPa) |
|---|---|---|
| 100 | 6.25 | 8.45 |
| 50 | 6.32 | 8.64 |
| 10 | 9.18 | 8.11 |
| 0 | 6.80 | 8.86 |

The fragmentation tests were conducted with the Minimat tensile machine, Polymer Laboratories Ltd. As a function of applied strain, the number of fibre ruptures and the debonding length developing from the ends of the fibre fragments were continuously monitored at the centre of the sample, in a region extending over 10 mm. Two parameters were computed using this data, namely the average fragment length, $L_{exp}$, and the average debonding ratio, $M_{exp}$. There are two methods for determining $L_{exp}$. The first, which consists of measuring the length of each individual fragment, is very tedious and requires the test to be stopped at specified values of applied strain. The second approach consists of dividing the length of the monitored region by the number of fibre ruptures increased by one. This procedure is fast, does not require the test to be stopped, and has been verified to produce accurate results [15]. The debonding ratio, $M_{exp}$, is the average portion of the fragment's length over which debonding has developed. For each monitored fragment, the total debonding length is measured optically and is reported to the fragment length; an average over multiple fragments (usually two or three) then produces an estimate of $M_{exp}$.

Fig. 8 summarizes the experimental results for the average aspect ratio, $S_{exp} = L_{exp}/d_f$, and the average debonding ratio, $M_{exp}$. At least five specimens were tested for each type of fibre; for clarity, only average values are reported. Table II gives the aspect ratio at saturation, $S_{sat}$, which is defined as the average fragment length at saturation reported to the fibre diameter.

It is concluded from the above experimental data that, with increasing levels of surface treatment, the strain of first rupture and the aspect ratio at saturation decrease; while debonding develops more slowly. The results of Fig. 8 constitute the main input to the proposed data reduction scheme.

TABLE II Average aspect ratio at saturation as a function of surface treatment

| SST (%) | 100 | 50 | 10 | 0 |
|---|---|---|---|---|
| $S_{sat}$ | 67 | 85 | 97 | 165 |

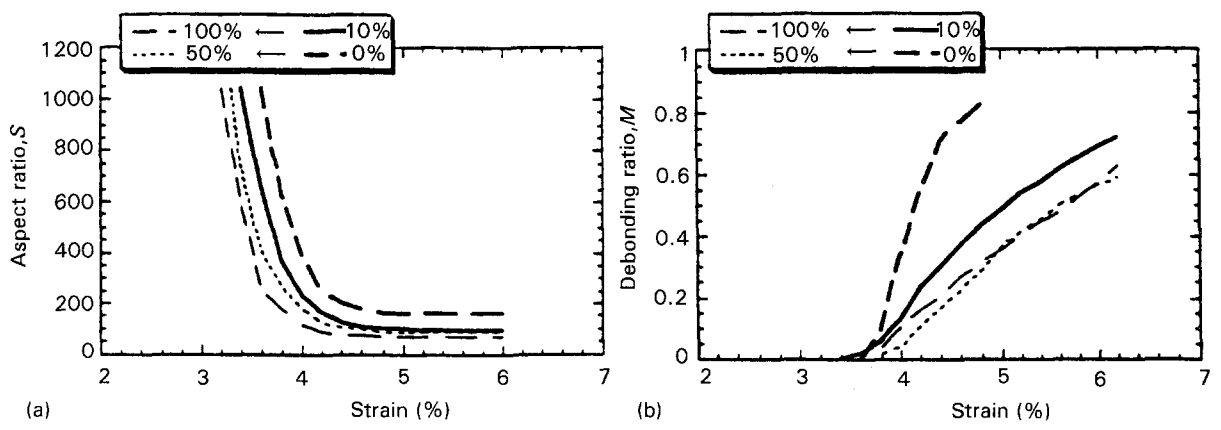


*Figure 8* (a) Average aspect ratio, and (b) debonding ratio as a function of applied strain and surface treatment.

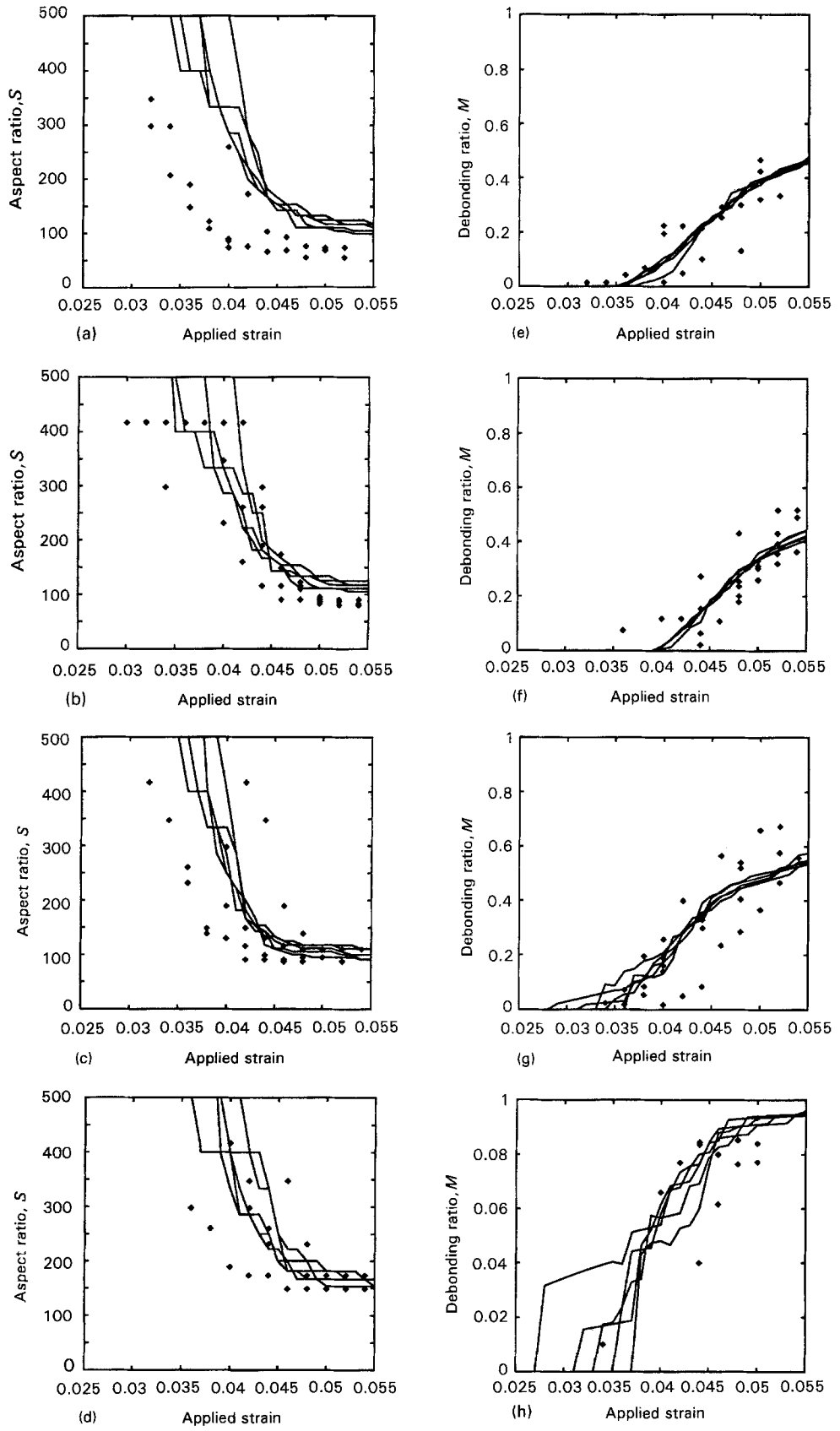


*Figure 9* Mean aspect ratio and debonding ratio as a function of applied strain for various levels of surface treatment ((a), (e) 100%; (b), (f) 50%; (c), (g) 10% and (d), (h) 0%). Comparison between experimental (◆) and simulation (——) results.

The fibres experience a compressive longitudinal residual stress, $\sigma_f^{res}$, due to shrinkage effects and crosslinking of the matrix during cooling. It is indeed observed experimentally that the strain at which the first fibre rupture occurs in the fragmentation specimen is higher than the critical strain of the isolated fibre. Correction for this delay yields the estimate $\sigma_f^{res} = -4.35$ GPa, which has been used in the simulations described below.

TABLE III Derived interface properties

| SST (%) | $\tau_{deb}$ (MPa) | $\tau_{fri}$ (MPa) |
|---|---|---|
| 100 | 174 | 26 |
| 50 | 187 | 19 |
| 10 | 141 | 42 |
| 0 | 54 | 25 |

TABLE IV Derived mean interface share stress according to Kelly's model

| SST (%) | 100 | 50 | 10 | 0 |
|---|---|---|---|---|
| $\tau_K$ (MPa) | 101 | 78 | 65 | 38 |

## 5. Results

The interfacial shear strength properties, $\tau_{deb}$ and $\tau_{fri}$, have been determined by applying the proposed data reduction scheme with the material and experimental data of Section 4. The values of $\tau_{deb}$ and $\tau_{fri} = c_1 + c_2\varepsilon$ that give the best agreement between experimental and simulated, $(S, \varepsilon)$ and $(M, \varepsilon)$, curves are determined on the basis of five different random generations of the fibre subsegment's strength. The results of this three-parameter optimization problem show that $c_1 \gg c_2\varepsilon$ for the studied materials, which implies that the derived values for $\tau_{fri}$ reduce to the constant $c_1$. Physically, this indicates that the differential Poisson's contraction plays a negligible role in the load transfer taking place at the interface, in comparison with the radial residual stress.

The final results for $\tau_{deb}$ and $\tau_{fri}$, computed as the averages of the interface properties obtained from the five optimization runs, are shown in Table III.

The simulation results for the five runs are compared to the experimental data in Fig. 9. Agreement is very good for the 0, 10 and 50% SST fibres. The results are less satisfactory for the 100% SST fibres, as far as the aspect ratio is concerned.

Although one should keep the limits of the proposed data reduction scheme in mind, the results are rich in information. First, Table III shows that the surface treatment increases the interfacial shear strength, $\tau_{deb}$. The highest value of $\tau_{deb}$, however, is obtained for the 50% SST fibres. Independent studies on the same materials, but based on the pull-out test, confirm this result [15]. Next, it is seen that surface treatment also influences the frictional resistance, $\tau_{fri}$, of the broken interface. The highest value is obtained for the 10% SST fibres. Finally, a high value of $\tau_{deb}$ does not necessarily imply a high value of $\tau_{fri}$. Thus, these two components of the interface mechanical behaviour are somewhat independent, and could be controlled separately by means of an appropriate surface treatment. This point is further addressed in a separate study [16], where the derived interfacial properties are related to the fibre's surface properties.

It is useful to compare the results of the proposed data reduction scheme to those obtained with the classical Kelly model. Here, the interface mechanical behaviour is characterized by a single parameter, $\tau_K$, given by

$$\tau_K = \frac{\overline{\sigma_f^{ult}}(l = S_{sat}d_f) - \sigma_f^{res}}{2S_{sat}} \quad (13)$$

Equation 13 is a modified version of the classical Kelly model [1], wherein the axial residual stress, $\sigma_f^{res}$, and the dependence of the mean fibre strength, $\overline{\sigma_f^{ult}}$, on length have been integrated. The latter is computed by means of Equation 10. The results are listed in Table IV.

The values of $\tau_K$ can be regarded as the mean interface shear stress at saturation. As expected, they lie between those shown in Table III for $\tau_{fri}$ and $\tau_{deb}$. According to the above interpretation of fragmentation data with the single parameter $\tau_K$, one would conclude that surface treatment increases the interface shear strength in a monotonic fashion. Clearly, information has been lost relative to that provided by the proposed data reduction scheme. Indeed, inspection of Table IV no longer reveals that the 50% level of surface treatment yields the best bond shear strength, while the 10% level is the optimum in terms of frictional resistance.

## 6. Conclusions

A new data reduction scheme for the fragmentation testing of polymer composites has been proposed. The input data are the stiffness and strength properties of the fibre and matrix, as well as the average fibre fragment and debonding ratios as a function of applied strain, measured during the fragmentation test. The interface mechanical properties are characterized by two independent parameters, namely the interface bond strength, $\tau_{deb}$, and the interface frictional resistance, $\tau_{fri}$. Derived values for $\tau_{deb}$ and $\tau_{fri}$ are determined by means of a simulation of the fragmentation test, in such a way that the difference between experimental and theoretical results for the fragment and debonding ratios is minimum.

This new scheme has been applied to carbon–epoxy systems with various levels of fibre surface treatment. The results show that surface treatment influences the two interface properties, $\tau_{deb}$ and $\tau_{fri}$, in different ways. This indicates the possibility of controlling $\tau_{deb}$ and $\tau_{fri}$ independently, thereby providing a rational route for tayloring the fibre–matrix interface in polymer composites.

## Acknowledgements

The graduate research of M. D. has been carried out in the framework of the EURAM programme N1IE-0047-C. The graduate research of Th. L. is partially supported by a grant from the *Fonds de Développement Scientifique* of the UCL. The results presented in this paper have been obtained within the framework of Interuniversity Attraction Poles initiated by the Belgian State, Prime Minister's Office, Science Policy Programming. The scientific responsibility rests with its authors.

## References


1. I. VERPOEST, M. DESAEGER and R. KEUNINGS, in "Controlled Interphases", edited by H. Ishida (Elsevier, Amsterdam, 1990) pp. 653–666.
2. C. GALIOTIS, R. J. YOUNG, P. H. J. YEUNG and D. N. BATCHELDER, *J. Mater. Sci.* **19** (1984) 3640.
3. I. M. ROBINSON, R. J. YOUNG, C. GALIOTIS and D. N. BATCHELDER, *ibid.* **22** (1987) 3642.
4. EI. M. ASLOUN, M. NARDIN and J. SCHULTZ, *ibid.* **24** (1989) 1835.
5. J-P. FAVRE and D. JACQUES, *ibid.* **25** (1990) 1373.
6. A. KELLY and G. J. DAVIES, *Metall. Rev.* **10** (1965) 20.
7. J-P. FAVRE, P. SIGETY and D. JACQUES, *J. Mater. Sci.* **26** (1991) 189.
8. M. R. PIGGOTT, "Load Bearing Fibre Composites" (Pergamon, Oxford, 1980) pp. 83–89.
9. T. LACROIX, B. TILMANS, R. KEUNINGS, M. DESAEGER and I. VERPOEST, *Comp. Sci. Technol.* **43** (1992) 379.
10. T. LACROIX, PhD thesis, Université Catholique de Louvain, Belgium, in preparation.
11. H. L. COX, *Brit. J. Appl. Phys.* **3** (1952) 72.
12. M. R. PIGGOTT, *J. Mater. Sci.* **13** (1978) 1709.
13. W. WEIBULL, *J. Appl. Mech.* **18** (1951) 293.
14. S. VAN DER ZWAAG, *J. Test. Eval.* **17** (1989) 292.
15. M. DESAEGER, PhD Thesis, Katholieke Universiteit Leuven, Belgium (1993).
16. M. DESAEGER, I. VERPOEST, H. T. CHEN, P. DENISON, F. JONES, T. LACROIX and R. KEUNINGS, in preparation (1994).



*Received 9 February*
*and accepted 6 July 1994*